

The ferroelectric transition in YMnO₃ from first principles

Craig J. Fennie and Karin M. Rabe

Department of Physics and Astronomy, Rutgers University, Piscataway, NJ 08854-8019

(Dated: August 6, 2018)

We have studied the structural phase transition of multiferroic YMnO₃ from first principles. Using group-theoretical analysis and first-principles density functional calculations of the total energy and phonons, we perform a systematic study of the energy surface around the prototypic phase. We find a single instability at the zone-boundary which couples strongly to the polarization. This coupling is the mechanism that allows multiferroicity in this class of materials. Our results imply that YMnO₃ is an improper ferroelectric. We suggest further experiments to clarify this point.

PACS numbers: 77.80.Bh, 61.50.Ks, 63.20.Dj

The hexagonal manganites, $ReMnO_3$ for $Re=Ho-Lu$ and Y , are a class of multiferroic materials that are simultaneously ferroelectric (FE) and antiferromagnetic (AFM).¹ In particular, YMnO₃ is FE at room temperature (RT) crystallizing in space group $P6_3cm$ (C_{6v} , $Z=6$).² Above $\approx 1270K$ it has been shown to undergo a transition to paraelectric (PE) $P6_3/mmc$ (D_{6h} , $Z=2$).^{3,4}

The sequence of phase transitions from the low temperature FE to the high temperature PE phase has been the subject of much debate. Based on pyroelectric measurements and lattice constants determined by x-ray diffraction, Ismailzade and Kizhaev argued that YMnO₃ undergoes a FE transition from $P6_3cm$ ($Z=6$) to an intermediate nonpolar $P6_3/mcm$ ($Z=6$) at $\approx 930K$.⁵ In contrast, Lukaszewicz and Karut-Kalicinska were unable from x-ray diffraction to resolve this intermediate nonpolar space group³ at 1005 K and saw no clear anomalies in the lattice constants at $\approx 930K$. Katsufuji et al. confirmed the latter results on the temperature dependence of the lattice constants and resolved the FE space group up to 1000K, the highest temperature they considered.⁶ The FE space group immediately below the zone-tripling transition is also supported by the structural refinements of Lonkai et al. on the closely related compounds $ReMnO_3$, for $Re = Lu, Tm, Yb$.⁷ On the other hand, Nénert et al. recently interpreted their x-ray diffraction measurements to support the observation of the intermediate $P6_3/mcm$ ($Z=6$) between 1020K and 1270K.⁴ The presence of some kind of feature at 930K is suggested by small anomalies in resistivity data at $\approx 950 K$ ⁸ (also observed in $HoMnO_3$ ⁹). Thus, the nature of the phase right below the 1270 K transition out of the PE phase, a precise characterization of the behavior around 900-1000 K, and the identification of the PE-FE transition in this material, remain subjects of great interest.

It has been established that to coexist with magnetism, the nature of the ferroelectricity cannot be that found in prototypical perovskite FEs such as $BaTiO_3$.¹⁰ Indeed, first-principles calculations have shown that the usual indicators of a FE instability (e.g. large Born effective charges) are absent in YMnO₃.¹¹ Polarization $\mathbf{P}_s = 6 \mu C/cm^2$ results from the tilting of the Mn-centered oxygen octahedra and buckling of the Y-O planes, with no significant off-centering of the Mn cations as would be

characteristic of a perovskite FE.¹¹ As such, YMnO₃ has been referred to as a “geometric ferroelectric.”¹² In this paper, we combine a group theoretical analysis of the experimental FE structure with first-principles calculations to describe the mechanism by which this “geometric ferroelectricity” originates. Computation of the coupling between a zone-boundary instability and a soft, but stable, zone-center phonon shows that it induces a low temperature $\mathbf{P}_s \approx 6.5 \mu C/cm^2$ consistent with experiments. Identifying this zone-boundary mode as the primary order parameter (OP), we argue that there is an improper FE transition in YMnO₃ at the observed zone-tripling transition, $\approx 1270K$. We suggest possible origins for the feature that has been observed around 1000K.

First-principles density-functional calculations using projector augmented-wave potentials were performed within the LSDA+U (local spin-density approximation plus Hubbard U) method¹³ as implemented in the *Vienna ab initio Simulation Package* (VASP).^{14,15} The wavefunctions were expanded in plane waves up to a kinetic energy cutoff of 500 eV. Integrals over the Brillouin zone were approximated by sums on a $4 \times 4 \times 2$ Γ -centered k -point mesh. Values of on-site Coulomb interaction $U = 8eV$ and exchange parameter $J=0.88eV$ were used for the Mn d-orbital as calculated by Ref. 16. Polarization was calculated using the modern theory of polarization¹⁷ as implemented in VASP. All results presented are within LSDA+U with A -type AFM order.¹¹ Calculations of phonons, structural energetics, and polarization were also performed within LSDA, and with both frustrated AFM¹⁶ and FM order; the results are essentially unchanged.

We performed full optimization of the lattice parameters and internal coordinates in the reported FE space group $P6_3cm$. As can be seen in Table I, excellent agreement with the experimental RT structure (lattice constants within $\approx 0.5\%$ and bond lengths within $\approx 1\%$ of the experimental values) is obtained.

Group theoretical analysis (e.g. Ref. 18,19) shows that there are three distinct symmetry-allowed phase transition sequences connecting the high-temperature prototypic phase, $P6_3/mmc$, to the low-temperature FE phase, $P6_3cm$, as shown in Fig. 1. There is a clear experimental consensus that the zone-tripling transition occurs be-

TABLE I: Crystal structure of ferroelectric YMnO₃, Space Group: $P6_3cm$, Exp. room temperature: $a=6.139\text{\AA}$, $c=11.41\text{\AA}$. LSDA+U: $a=6.099\text{\AA}$, $c=11.42\text{\AA}$

Atom	Exp. Ref.2			LSDA+U		
Y ₁ (2a)	0	0	0.2743	0	0	0.2751
Y ₂ (4b)	$\frac{1}{3}$	$\frac{2}{3}$	0.2335	$\frac{1}{3}$	$\frac{2}{3}$	0.2313
Mn (6c)	0.3352	0	0.0000	0.3334	0	0.0000
O _{ap(1)} (6c)	0.3083	0	0.1627	0.3058	0	0.1642
O _{ap(2)} (6c)	0.3587	0	-0.1628	0.3601	0	-0.1641
O _{eq(3)} (2a)	0	0	-0.0218	0	0	-0.0242
O _{eq(4)} (4b)	$\frac{1}{3}$	$\frac{2}{3}$	0.0186	$\frac{1}{3}$	$\frac{2}{3}$	0.0207

fore or at the FE transition, thereby excluding $P6_3mc$ as an intermediate phase and ruling out path (1). In principle, path (2) could account for both the observed zone-tripling transition at 1270K and a possible second transition at ≈ 1000 K. This transition sequence would be a first-order transition to the non-polar intermediate phase (by the freezing-in of a K_1 phonon), followed by a second-order, proper FE transition to the RT phase (due to a softening of an infrared-active phonon). Path (3) describes a second-order transition out of the prototypic phase, by the freezing-in of a K_3 phonon, directly to the FE space group. Unlike what has been proposed in the literature⁷, Path (3) does not require a second transition to account for FE order (as discussed below).²⁰

Independent of the path,²¹ the distortion that relates the prototypic phase to the low temperature FE phase can be decomposed into the symmetry-adapted modes of the prototypic phase as follows: Γ_2^- (zone-center polar mode), K_1 and K_3 (zone-boundary modes at $q=\frac{1}{3}, \frac{1}{3}, 0$), and Γ_1^+ (the identical representation).^{22,23} This decomposition is shown in Table II for the experimental RT structure. The excellent agreement between theory and experiment for the structure, Table I, results in similar agreement for the mode decomposition.

The relative strength of each mode in the FE structure may be quantified by considering its amplitude,²⁴ Q , also given in Table II. We find, as did previous first-principles calculations and structural analysis,¹¹ that the FE structure is dominated by the K_3 mode, with Y and O_{eq} atoms undergoing the largest displacements. The relative sizes of the symmetry-adapted mode amplitudes in the RT FE phase offer a valuable clue to which of the three phase-transition paths is taken by YMnO₃. In soft-mode driven structural transitions one expects a mode that stabilizes an intermediate phase at higher temperatures to be at least comparable in strength (not necessarily the largest) to any other modes appearing in the lower temperature phase. If Q_{K_1} were the primary structural distortion out of the prototypic phase, it should be retained through the second transition into the low temperature FE phase, which is not the case in YMnO₃. Thus path (2) tends to be ruled out by the smallness of Q_{K_1} . Finally, we consider the remaining possibility, path (3). The fact that

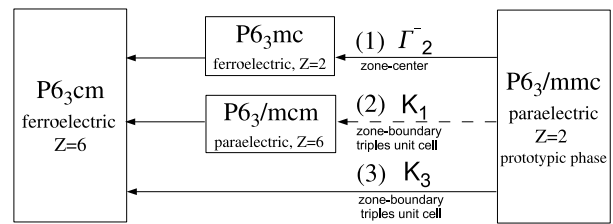


FIG. 1: Group-subgroup sequence of allowed phase transitions connecting the high-temperature prototypic phase, $P6_3/mmc$, to the low-temperature ferroelectric phase, $P6_3cm$. Each sequence is labeled by an irrep of the prototypic phase where structural distortions associated with these irreps determine possible intermediate phases.

Q_{K_3} is one to two orders of magnitude larger than $Q_{\Gamma_2^-}$ and Q_{K_1} respectively, suggests that Q_{K_3} is in fact the primary structural distortion out of the prototypic phase (e.g Ref. 21) and thus that YMnO₃ follows path (3).

First principles ($T=0$) investigation of the phonons and the structural energetics around the prototypic phase also shows path (3) to be the most likely scenario. For the structural parameters of the prototypic phase, we used the minimum energy structure within $P6_3/mmc$: $a=6.168\text{\AA}$, $c=11.23\text{\AA}$ and $u_{O_{ap}}=0.9166$. This corresponds to a nearly homogeneous compression of the lattice constants by about 1.4% compared with those measured by Lukasewicz at 1280K, an underestimate typical of LSDA calculations. Phonons at the Γ and K -point in the Brillouin zone of the prototypic phase were computed by constructing the relevant block of the dynamical matrix from Hellmann-Feynman forces. This allowed us to greatly reduce the number of calculations and provided higher numerical accuracy in the determination of the force-constant eigenvectors. At the Γ -point we find that the three infrared-active Γ_2^- phonons are stable with the lowest frequency Γ_2^- (TO1): $\omega = 90 \text{ cm}^{-1}$. At the K -point, we computed the three K_3 phonons by a similar

TABLE II: Decomposition of Exp. Ref. 2 atomic displacements (\AA) into symmetry-adapted modes of prototypic $P6_3/mmc$. Mode amplitudes, Q , are shown in \AA .

	Γ_2^-	K_1	K_3	
	[001]	[100]	[100]	[001]
Y ₁	-0.038	0	0	0.310
Y ₂	-0.038	0	0	-0.155
Mn	-0.005	0.011	0	0
O _{ap(1)}	-0.005	0.001	-0.155	0
O _{ap(2)}	-0.005	0.001	0.155	0
O _{eq(3)}	0.054	0	0	-0.307
O _{eq(4)}	0.054	0	0	0.153
Q_{exp}	0.16	0.03	0.93	
Q_{theory}	0.19	0.01	1.00	

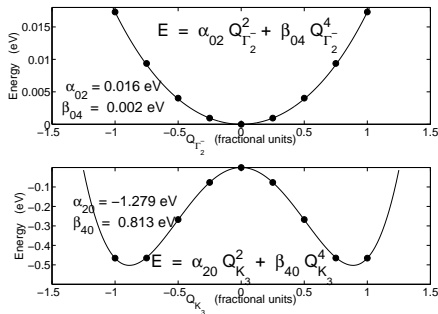


FIG. 2: Energy as a function of (top) $Q_{\Gamma_2^-}$ and (bottom) Q_{K_3} .

method and found one highly unstable mode $K_3(1)$: $\omega = i 153 \text{ cm}^{-1}$. In contrast, both K_1 phonons are quite stable with $K_1(1)$: $\omega = 264 \text{ cm}^{-1}$ and $K_1(2)$: $\omega = 522 \text{ cm}^{-1}$. Since lattice instabilities are known in some cases to be sensitive to volume, we repeated these calculations at the experimental lattice constants; the results are qualitatively unchanged.

The stability of the Γ_2^- and K_1 modes is additional evidence to rule out paths (1) and (2), respectively. Admittedly, as these are $T=0$ calculations there is still a possibility that an intermediate phase could be stabilized by an anomalous entropic contribution to the free energy at finite temperatures,²⁵ so that, e.g. $P6_3/mcm$ would be more stable than $P6_3cm$ for a range of temperatures below 1270K. However, in light of the strength of the K_3 instability and as we will show, the associated energy scale, the transition out of the PE phase is most naturally driven by the K_3 mode, corresponding to path (3).

We can understand how the $K_3(1)$ zone-boundary instability produces a polarization by calculating the energy surface around the prototypic phase as a function of the relevant modes. To simplify the analysis, the fact that all Γ_1^+ and K_1 phonons are stable in the prototypic phase and contribute very little to the total structural distortion suggests that the coupling of these modes to $K_3(1)$ will be small and can be ignored. Within this reduced subspace we expand the energy of the crystal including all symmetry allowed terms to fourth order in Q_{K_3} and $Q_{\Gamma_2^-}$ to obtain:

$$\mathcal{F}(Q_{K_3}, Q_{\Gamma_2^-}) = \alpha_{20} Q_{K_3}^2 + \alpha_{02} Q_{\Gamma_2^-}^2 + \beta_{40} Q_{K_3}^4 + \beta_{04} Q_{\Gamma_2^-}^4 + \beta_{31} Q_{K_3}^3 Q_{\Gamma_2^-} + \beta_{22} Q_{K_3}^2 Q_{\Gamma_2^-}^2 \quad (1)$$

Next we performed a series of first-principles calculations where we freeze-in various amplitudes of Q_{K_3} and $Q_{\Gamma_2^-}$ and compute the total energy. The energy expansion, Eq. 1, was then fit using only six data points, yielding excellent agreement with the remaining ~ 20 data points. As we will show, the model energy fits the calculated data well over the entire energy surface, justifying our truncation of the Taylor expansion to fourth order.

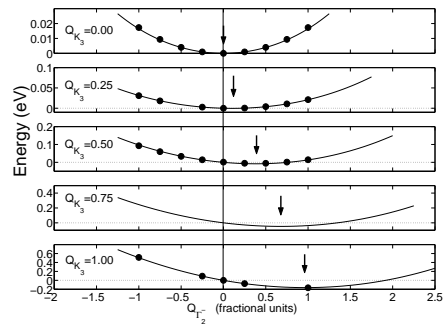


FIG. 3: Energy as a function of $Q_{\Gamma_2^-}$ at fixed Q_{K_3} .

In Fig. 2 we show the total energy (of the 30-atom cell) as a function of the $Q_{\Gamma_2^-}$ (top) and Q_{K_3} (bottom) fractional displacements. As expected, the Γ_2^- mode is stable while the double-well potential of the K_3 mode is apparent. The coupling between the modes can be seen by plotting the energy as a function of $Q_{\Gamma_2^-}$ at fixed Q_{K_3} as in Fig. 3. Notice that once Q_{K_3} becomes non-zero the equilibrium position of $Q_{\Gamma_2^-}$ (indicated by the arrow) shifts to a positive value and continues to increase with increasing Q_{K_3} . Also as Q_{K_3} increases, the curvature of the energy increases due to the $\beta_{22}=0.155 \text{ eV}$ term which renormalizes the quadratic coefficient of $Q_{\Gamma_2^-}$. The effect of the K_3 mode is not to decrease the stability of the Γ_2^- mode, but rather to “push” the Γ_2^- mode to a non-zero equilibrium position, playing a role analogous to that of a field. This “geometric field” is the mechanism for ferroelectricity in the hexagonal manganites.²⁶ Further, the strong $\beta_{31}=-0.334 \text{ eV}$ coupling between the $K_3(1)$ and Γ_2^- (TO1) lattice modes, i.e. phonons, is responsible for the comparatively large value of $\mathbf{P}_s \approx 6 \mu\text{C}/\text{cm}^2$. Indeed, if this coupling were to be turned off, the polarization generated by $K_3(1)$ (coupling only to the electronic density) is reduced to $\mathbf{P}_s \approx 0.1 \mu\text{C}/\text{cm}^2$.²⁷

Now let us return to the discussion of the PE-to-FE path. If we now identify $K_3(1)$ as the primary OP and Γ_2^- (TO1) as a secondary OP, inspection of Fig. 3 reveals interesting crossover behavior of the Γ_2^- mode. Minimizing the free energy over $Q_{\Gamma_2^-}$ leads to two cases:

$$\text{Region 1: } Q_{K_3} \ll \sqrt{\left| \frac{\alpha_{02}}{\beta_{22}} \right|} \implies Q_{\Gamma_2^-} \propto -\frac{\beta_{31}}{2\alpha_{02}} Q_{K_3}^3$$

$$\text{Region 2: } Q_{K_3} \gg \sqrt{\left| \frac{\alpha_{02}}{\beta_{22}} \right|} \implies Q_{\Gamma_2^-} \propto -\frac{\beta_{31}}{2\beta_{22}} Q_{K_3}$$

Since the polarization, \mathbf{P} , is a first order polar tensor it has the same transformation properties as the symmetry-adapted Γ_2^- mode, i.e. $\mathbf{P} \propto Q_{\Gamma_2^-}$. Using the modern theory of polarization we can calculate the polarization as a function of the structural Γ_2^- mode. The physical quantity of interest though is the polarization as a function of the primary OP, Q_{K_3} , which we show in Fig. 4. As the K_3 structural distortion is initiated, \mathbf{P}_s becomes non-zero but is small due to the $Q_{K_3}^3$ dependence until the emergence of a crossover to $\mathbf{P}_s \propto Q_{K_3}$. This leads to an apparent “turn-on” at a finite value of Q_{K_3} . We calcu-

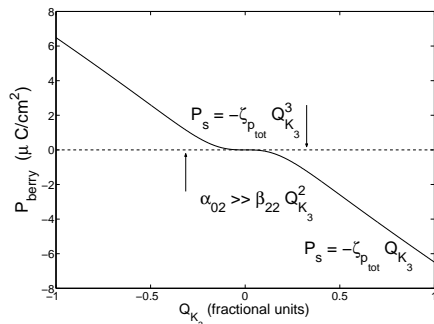


FIG. 4: Polarization, \mathbf{P}_s , vs. primary order parameter, Q_{K_3} .

late the total energy (per formula unit) lowering from the PE to FE to be $\mathcal{O}(1000\text{K})$ (the precise value fortuitously being 1240K) and the width of this crossover region to be $\mathcal{O}(100\text{K})$.

In this paper, we have shown that the overwhelming weight of the experimental and theoretical evidence supports path (3), with an improper FE transition out of the high-temperature PE phase at 1270K . The $K_3(1)$ phonon is strongly unstable and couples to the $\Gamma_2^-(\text{TO1})$ phonon leading to the observed polarization. The unusual dependence of the polarization on the primary order parameter would lead to a broadened pyroelectric peak lower than T_c and could, through coupling to strain,

lead to an isostructural, FE-to-FE, transition, although this last point is only speculative. This differs from previous models⁷ in that YMnO_3 is already polar when this isostructural transition occurs. An additional intriguing possibility to explain the apparent lower temperature transition is that, due to the presumably inhomogeneous nature of K_3 near T_c (which we have been assuming to be homogeneous), fluctuations suppress the coupling between $K_3(1)$ and $\Gamma_2^-(\text{TO1})$ till some temperature lower than T_c , this second transition temperature likely being sample dependent.²⁸ In this scenario, the path to the FE phase is still along (3), but the $\text{P6}_3\text{cm}$ phase in the intermediate temperature range would be paraelectric in an average sense, as originally suggested by Lukaszewicz and Karut-Kalicinska.³ Clearly, further theoretical and experimental work is necessary to characterize the lower temperature isostructural transition and the nature of the polarization in the intermediate phase. Finally, it should be appreciated, that regardless of the actual path taken, the softening of the K_3 mode sets up a “geometric field” that induces a substantial polarization, thus providing a mechanism to achieve multiferroicity in the hexagonal manganites.

Useful discussions with S-W. Cheong, D.R. Hamann, G. Néner, T. Palstra, A. Sushkov, and D.H. Vanderbilt are acknowledged. This work was supported by NSF-NIRT Grant No. DMR-0103354.

- ¹ S.C. Abrahams, *Acta Cryst. B* **57**, 485 (2001).
- ² B.B. VanAken, A. Meetsma, and T.T.M. Palstra, *Acta Cryst. C* **57**, 230 (2001); cond-mat/0106298.
- ³ K. Lukaszewicz and J. Karut-Kalicinska, *Ferroelectrics* **7**, 81 (1974).
- ⁴ G. Néner, Y. Ren, H.T. Stokes, and T.M. Palstra, cond-mat/0504546.
- ⁵ I.G. Ismailzade and S.A. Kizhaev, *Sov. Phys. Solid State* **7**, 236 (1965).
- ⁶ T. Katsufuji, M. Masaki, A. Machida, M. Moritomo, K. Kato, E. Nishibori, M. Takata, M. Sakata, K. Ohoyama, K. Kitazawa, and H. Takagi, *Phys. Rev. B* **66**, 134434 (2002).
- ⁷ Th. Lonkai, D.G. Tomuta, U. Amann, J. Ihringer, R.W.A. Hendrikx, D.M. Többens, and J.A. Mydosh, *Phys. Rev. B* **69**, 134108 (2004).
- ⁸ T. Katsufuji, S. Mori, M. Masaki, Y. Moritomo, N. Yamamoto, and H. Takagi, *Phys. Rev. B* **64**, 104419 (2001).
- ⁹ From $\partial_T \ln(\rho)$ and thermal hysteresis, private communication, S.M. Yeo and S-W. Cheong.
- ¹⁰ N.A. Hill, *J. Phys. Chem. B*, **104**, 6694 (2000).
- ¹¹ B.B. VanAken, T.T.M. Palstra, A. Filippetti, and N.A. Spaldin, *Nature Materials* **3**, 164 (2004).
- ¹² C. Ederer and N.A. Spaldin, *Nature Materials* **3**, 849 (2004).
- ¹³ V.I. Anisimov, J. Zaanen, and O.K. Andersen, *Phys. Rev. B* **44**, 943 (1991).
- ¹⁴ G. Kresse and J. Hafner, *Phys. Rev. B* **47**, R558 (1993); G. Kresse and J. Furthmüller, *ibid.* **54**, 11169 (1996).
- ¹⁵ P.E. Blöchl, *Phys. Rev. B* **50**, 17953 (1994); G. Kresse and D. Joubert, *ibid.* **59**, 1758 (1999).
- ¹⁶ J.E. Medvedeva, V.I. Anisimov, M.A. Korotin, O.N. Mryasov, and A.J. Freeman, *J. Phys.: Condens. Matter* **12**, 4947 (2000).
- ¹⁷ R.D. King-Smith and D. Vanderbilt, *Phys. Rev. B* **47**, R1651 (1993).
- ¹⁸ H.T. Stokes and D. M. Hatch (2002). ISOTROPY <http://stokes.byu.edu/isotropy.html>
- ¹⁹ Bilbao Crystall. Server: <http://www.cryst.ehu.es>
- ²⁰ H.T. Stokes and D. M. Hatch, *Phase Transitions* **34**, 53 (1991).
- ²¹ J.M. Pérez-Mato, M. Aroyo, A. García, P. Blaha, K. Schwarz, J. Schweifer, and K. Parlinski, *Phys. Rev. B* **70**, 214111 (2004).
- ²² J.M. Pérez-Mato, J.L. Mañes, M.J. Tello, and F.J. Zúñiga, *J. Phys. C: Solid State Phys.* **14**, 1121 (1981).
- ²³ J.L. Mañes, M.J. Tello, and J.M. Pérez-Mato, *Phys. Rev. B* **26**, 250 (1982).
- ²⁴ We normalize to the 30-atom cell. For experimental structure, $Q_{\Gamma_1^+}=0$ by construction (see e.g. H.T. Stokes, C. Sadate, D. M. Hatch, L.L. Boyer, and M.J. Mehl, *Phys. Rev. B* **65**, 064105 (2002).) From our first-principles calculations, $Q_{\Gamma_1^+}=0.03\text{\AA}$.
- ²⁵ M.T. Dove, *Structure and Dynamics* (Oxford University Press, Oxford, 2003).
- ²⁶ Using DFT-SIC method, the first-principles study of Ref. 11 found the total Γ structural distortion, i.e. $\Gamma_2^- +$

Γ_1^+ independently unstable. It should be emphasized, the essential physics of the geometrical field is the coupling between the Γ_2^- and K_3 modes and does not depend on the stability of the Γ_2^- mode.

²⁷ C.J. Fennie and K.M. Rabe, unpublished.

²⁸ D.R. Hamann, private communication.